Influences of (Pr, Mn) Dopants Ratios on Crystal Structure, Optical, and Electrical Characteristics of BiFeO_3

Iriani, Yofentina
Department of Physics, Faculty of Mathematics and Sciences, Universitas Sebelas Maret

Mercyurita Dewi Noviastuti
Department of Physics, Faculty of Mathematics and Sciences, Universitas Sebelas Maret

Suryana, Risa
Department of Physics, Faculty of Mathematics and Sciences, Universitas Sebelas Maret

Dianisa Khoirum Sandi
Department of Physics, Faculty of Mathematics and Sciences, Universitas Sebelas Maret

他

https://doi.org/10.5109/7236874

出版情報：Evergreen. 11 (3), pp.2317-2323, 2024-09. Interdisciplinary Graduate School of Engineering Sciences, Kyushu University, Japan
バージョン：

Influences of (Pr, Mn) Dopants Ratios on Crystal Structure, Optical, and Electrical Characteristics of $BiFeO_3$

Yofentina Iriani[1,*], Mercyurita Dewi Noviastuti[1], Risa Suryana[1], Dianisa Khoirum Sandi[1], Didier Fasquelle[2]

[1]Department of Physics, Faculty of Mathematics and Sciences,
Universitas Sebelas Maret, Jl. Ir. Sutami 36 A Kentingan Surakarta, 57126, Indonesia

[2]Department of Unitede Dynamique et Structure des Materiaux Moleculaires,
Universite du Littoral Cote d'Opale, CS 80699F-62228 Calais, France

*Author to whom correspondence should be addressed:
E-mail: yofent_iriani@staff.uns.ac.id

(Received October 28, 2023; Revised September 2, 2024; Accepted September 7, 2024).

Abstract. Bismuth ferrite ($BiFeO_3$) is a single-phase multiferroic material demonstrating magnetic (antiferromagnetic) and ferroelectric natures at room temperature. Here, $BiFeO_3$ and $Bi_{1-x}Pr_xFe_{1-y}Mn_yO_3$, where (x, y= 0%-20%), have been synthesized by means of Chemical Solution Deposition (CSD) technique and grown on quartz substrates via spin coater. This research aimed to identify the effects of mole variation of Praseodymium (Pr) and Manganese (Mn) dopants on the crystal structure and optical and electrical characteristics of $BiFeO_3$ and $Bi_{1-x}Pr_xFe_{1-y}Mn_yO_3$. According to the X-ray diffraction (XRD) data, adding (Pr, Mn) dopants into $BiFeO_3$ caused a shift in the diffraction angle toward smaller angles. As a result, the unit cell volume, lattice parameters, and crystal size reduced with the increasing number of (Pr, Mr). Next, according to the UV-Vis Spectrophotometer data, the addition of (Pr, Mn) dopants could decrease the transmittance and increase the absorbance, so the refractive index decreased while the light dispersion increased. Moreover, the increase in the (Pr, Mn) concentration ratio could enhance I-V characteristics of (Pr, Mn) co-doped $BiFeO_3$. Hence, it could be concluded that adding more (Pr, Mn) concentration ratios improved the crystal structure and optical and electrical characteristics of (Pr, Mn) co-doped $BiFeO_3$.

Keywords: (Pr, Mn) co-doped $BiFeO_3$; structural characteristic; optical characteristic; electrical characteristic

1. Introduction

Alternative and renewable energy fields have undergone significant development in the last decade. Of the several alternative energy sources, solar energy is one of the most critical resources from nature[1,2]. Solar energy conversion into electrical energy by photovoltaic (PV) is globally recognized. Photovoltaics is the most promising alternative energy source, relying on the material, mechanism, and conversion efficiency[3]. Multiferroic materials are a new field of study in photovoltaic (PV) manufacturing and are attracting attention due to their high photon energy responsiveness and suitability for photovoltaic applications[4].

Bismuth ferrite ($BiFeO_3$) is an intriguing multiferroic material owing to its high ferroelectric Currie temperature (T_C = 830°C) and antiferromagnetic Neel temperature (T_N = 370°C)[5]. In the $BiFeO_3$ material, ferroelectricity is produced by Bi^{3+} ions, while antiferromagnetic is caused by Fe^{3+} ions[6]. It is also an eco-friendly multiferroic material possessing a narrow bandgap of ~ 2.2 – 2.7 eV and large remnant polarization of 90 μC/cm^2, making it suitable for photovoltaic device applications[3,7]. Furthermore, this material exhibits both bandgap-based photovoltaic and bulk-based photovoltaic effects due to its polarization-based charge transport mechanism[5,7]. Therefore, these advantages can be applied to higher photovoltaic efficiency if the short-circuit current density is also increased[8]. Even though having attractive physical properties, BFO has several disadvantages, such as large leakage current density, low dielectric constants, high loss tangents, and the formation of complex phases because of the volatile nature of bismuth[8,9,10]. These aspects prevent its applicability to device fabrication.

Over the years, researchers have worked with strategies to fix these problems and improve BFO performance. Of the strategies, doping at Bi-site, Fe-site, or Bi-Fe-sites is the most effective, straightforward, and extensively studied. Studies have reported that doping at Bi-site with rare earth ions, including Pr, Eu, Gd, La, Sm, Nd, etc., could control bismuth volatility, thereby reducing oxygen vacancy and further declining leakage density [11-18].

Meanwhile, the doping at the Fe-site with transition metals, such as Co, Cr, Mn, Ni, Ru, etc., could fill the oxygen vacancies, thereby decreasing the leakage current[16,19-25]. Other studies also demonstrated that ions doping at Bi-site, Fe-site, or Bi-Fe-sites of BFO caused the optical and multiferroic properties to improve[17,23-25].

Pattanayak et al. have also exposed increasing dielectric constant and decreasing tangent loss due to Pr doping in the Bi-site[9]. Iriani et al. have reported that Pr doping in the Bi-site of BFO enhanced its optical characteristics[10]. Xia-Li et al. showed that fabricated Mn-doped BFO demonstrated an excellent remnant polarization (312 μC/cm^2) and a low leakage current[19]. Sajjad et al. exhibited the enhancement of structural property and decrement of bandgap energy of Mn-doped BFO nanoparticles[23].

The co-doping at the Bi-Fe-sites can be more advantageous due to the combination of two dopants in both sites to achieve better performance. The synthesis of co-doped $BiFeO_3$ is challenging and still requires more attention, predominantly using the CSD fabrication method and investigating the optical properties. CSD can efficiently control the material composition and obtain a highly transparent optical film[26,27]. Therefore, in this study, $BiFeO_3$ and Pr-Mn co-doped $BiFeO_3$ ($Bi_{1-x}Pr_xFe_{1-y}Mn_yO_3$) was done with the variation of Pr(x)/Mn(y) ratios of (x, y = 0.03, 0.03; 0.03, 0.05; 0.05, 0.03 and 0.05, 0.05) via the CSD technique. The study aimed to identify the effects of the (Pr, Mn) concentration ratios on the crystal structure and optical and electrical characteristics of $Bi_{1-x}Pr_xFe_{1-y}Mn_yO_3$.

2. Experimental details

This research was conducted from January to July 2022 at the Materials Laboratory of Physics Study Program and Integrated Laboratory of the Faculty of Mathematics and Natural Sciences (FMIPA), Sebelas Maret University (UNS).

2.1 Materials and Synthesis

$BiFeO_3$ and $Bi_{1-x}Pr_xFe_{1-y}Mn_yO_3$ films were fabricated via the CSD technique. The starting materials involved $Bi(NO_3)_3.5H_2O$ (Sigma Aldrich, ≥99.9%), $Fe(NO_3)_3.9H_2O$ (Sigma Aldrich, ≥99.9%), $Pr(NO_3)_3.6H_2O$ (Sigma Aldrich, ≥99.9%), and $Mn(NO_3)_3.6H_2O$ (Sigma Aldrich, ≥99.9%) as the Bi, Fe, Pr, and Mn source, respectively; acetic acid (CH_3CO_2H) (Sigma Aldrich, ≥99,7%) and 2-methoxy ethanol ($C_3H_8O_2$) (Sigma Aldrich, ≥99,8%) as the solvents; and acetylacetone (Sigma Aldrich, ≥99,3%) as the stabilizer agent. First, the materials were balanced following their chemical compositions where the molar concentrations of Pr (x) and Mn (y) were varied at (x, y = 0%-20%). Afterward, they were mixed until homogenous. The solutions of $BiFeO_3$ and $Bi_{1-x}Pr_xFe_{1-y}Mn_yO_3$ were then coated on quartz substrates. The coating was done by a spin coater at 3000 rpm for 30 seconds. Next, annealing was done on the samples at 600^{o}C for 4 h.

2.2 Characterization

The samples were characterized via XRD (Philips PW 3710/40 kV) with Cu Ka radiation (λ = 1.5406 Å) to determine the crystal structure, UV-Vis spectrophotometer (Lambda 25) to identify the optical properties, and *I-V* meter (Keithley 2602A) to investigate the electrical properties.

The data from the XRD tested was analyzed using a refinement process by Rietveld analysis using GSAS software, resulting in the crystal structure information. Besides, the crystal structure information, including the lattice constant and crystallite size, was also calculated manually. The lattice constant of $Bi_{1-x}Pr_xFe_{1-y}Mn_yO_3$ can be computed using Equation 1[28-30].

$$\frac{1}{d^2} = \frac{4}{3}\left(\frac{h^2+hk+k^2}{a^2}\right) + \frac{l^2}{c^2} \quad (1)$$

d is the distance between planes in Miller indices (*hkl*), and *a*, *b,* and *c* are lattice constants. The crystallite size of $Bi_{1-x}Pr_xFe_{1-y}Mn_yO_3$ was determined with the Scherrer equation[29-30].

$$D = \frac{k\lambda}{\beta_D \cos\theta} \quad (2)$$

$$\beta_D^2 = \left[\beta^2{}_{measured} - \beta^2{}_{\text{instrumental}}\right] \quad (3)$$

$$D = \frac{k\lambda}{\beta_D \cos\theta} = \cos\theta \frac{k\lambda}{D}\left(\frac{1}{\beta_D}\right) \quad (4)$$

Where *D* is the crystallite size (nm), λ is the wavelength (1.54056 Å), *k* is a constant of 0.94, β_D is the full width at half-maximum (FWHM), and θ is the peak position.

Next, the samples were characterized via a UV-Vis spectrophotometer to obtain the absorbance (*A*) and transmittance (*T%*). They were then exploited to determine the index of refraction of $Bi_{1-x}Pr_xFe_{1-y}Mn_yO_3$ using Equation 5-7[31-32].

$$n = \left[N_1 + (N_1^2 - s^2)^{\frac{1}{2}}\right]^{\frac{1}{2}} \quad (5)$$

$$N_1 = \frac{2s}{T_m} + \frac{s^2+1}{2} \quad (6)$$

$$S = \frac{2s}{T_m} + \sqrt{\frac{1}{T_s^2} - 1} \quad (7)$$

Where *S* is a transmission spectrum, N_1 is a spectral region, T_S is the substrate transmission, T_m is a transmission of samples, and *n* is the index of refraction. The relation between the refractive index and photon energy can be determined by the following formula[30,31].

$$n^2(E) = 1 + \frac{E_m E_d}{E_m^2 - E^2} \quad (8)$$

$$\frac{1}{n^2-1} = \frac{E_o}{E_d} - \left(\frac{1}{E_o E_d}\right) E^2 \quad (9)$$

$$E2 = (h\nu)^2 \quad (10)$$

Where E_o is oscillator energy, E_d is dispersion energy, hc=1.9865x10^{-25} kg m^3/s^2, λ is the wavelength, $E_m = E_o$, and $h\nu = hc/\lambda$.

3. Results and discussion

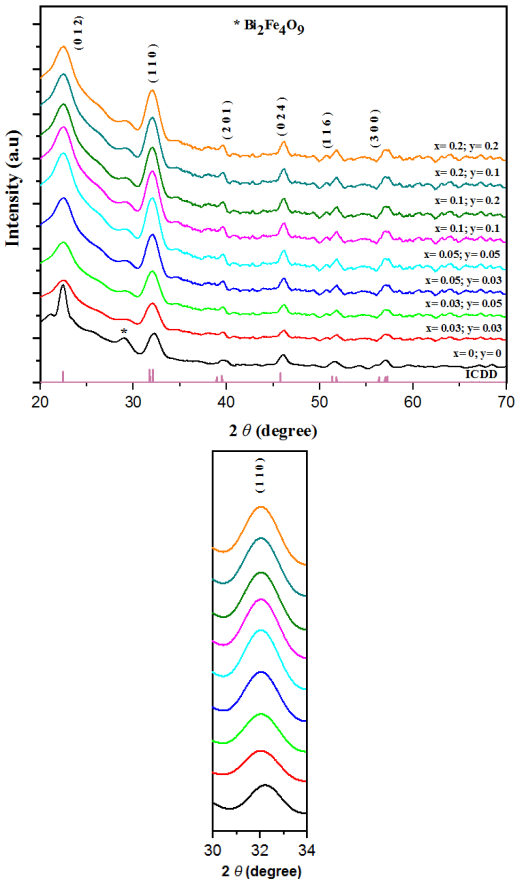

Fig. 1: (left) Diffraction patterns of $BiFeO_3$ and $Bi_{1-x}Pr_xFe_{1-y}Mn_yO_3$, and (right) magnification of (110) peaks.

Figure 1a presents the diffraction profiles of the $BiFeO_3$ and $Bi_{1-x}Pr_xFe_{1-y}Mn_yO_3$ samples. The $BiFeO_3$ pattern reveals the emergence of the impurity phase ($BiFe_4O_9$). The emergence of this phase is due to the crystal formation not perfectly occurring during the annealing process. It is considered that since the melting of Bi is 271.4°C, part of Bi's atoms evaporates during the thermal process, increasing the Fe amount. It leads to the formation of other phases or impurities[33]. Based on Fig. 1b, adding more (Pr, Mn) concentration causes a shift in the diffraction angles toward smaller angles.

The shift is due to the Pr dopant (r = 1.13 Å) substituting Bi – site (r = 1.17 Å) has a smaller atomic radius[34], and Mn (r = 0.48 Å) dopant substituting Fe – site (r = 0.645 Å) also has a smaller atomic radius. The substitution shrinks the unit cell volume of the materials. The smaller unit cell volume leads to a smaller atomic distance, shifting the diffraction angles[35], and indicates the smaller lattice constant, as shown in Table 1. The lattice parameters were attained as of the refinement process by GSAS software with Rietveld analysis and manual calculation (Eq.1). The slightly different lattice parameters from both methods might be due to the instrument factor in GSAS software.

Table 1. Lattice parameters, crystallite size, and lattice strain of $BiFeO_3$ and $Bi_{1-x}Pr_xFe_{1-y}Mn_yO_3$

Samples	GSAS Refinement		Calculation		Crystallite size (nm)	Lattice strain
	a=b (Å)	c (Å)	a=b (Å)	c (Å)		
$BiFeO_3$	5.577	13.861	5.578	13.879	26.29	0.016
$Bi_{0.97}Pr_{0.03}Fe_{0.97}Mn_{0.03}O_3$	5.574	13.857	5.577	13.867	20.25	0.023
$Bi_{0.97}Pr_{0.03}Fe_{0.95}Mn_{0.05}O_3$	5.572	13.852	5.576	13.867	20.19	0.023
$Bi_{0.95}Pr_{0.05}Fe_{0.97}Mn_{0.03}O_3$	5.572	13.852	5.576	13.867	20.03	0.023
$Bi_{0.95}Pr_{0.05}Fe_{0.95}Mn_{0.05}O_3$	5.572	13.852	5.576	13.867	19.87	0.023
$Bi_{0.9}Pr_{0.1}Fe_{0.9}Mn_{0.1}O_3$	5.571	13.848	5.574	13.861	16.80	0.023
$Bi_{0.9}Pr_{0.1}Fe_{0.8}Mn_{0.2}O_3$	5.571	13.848	5.574	13.861	16.66	0.023
$Bi_{0.8}Pr_{0.2}Fe_{0.9}Mn_{0.1}O_3$	5.571	13.850	5.572	13.857	16.55	0.024
$Bi_{0.8}Pr_{0.2}Fe_{0.8}Mn_{0.2}O_3$	5.572	13.848	5.571	13.857	16.52	0.024

Table 2. I-V characteristics of $BiFeO_3$ and $Bi_{1-x}Pr_xFe_{1-y}Mn_yO_3$

Samples	I_{sc} (A)	V_{oc} (V)	FF	Eff (%)
$BiFeO_3$	-0.00010	0.1816	0.2914	0.0061
$Bi_{0.97}Pr_{0.03}Fe_{0.97}Mn_{0.03}O_3$	-0.00013	0.1818	0.4470	0.0136
$Bi_{0.97}Pr_{0.03}Fe_{0.95}Mn_{0.05}O_3$	-0.00014	0.1818	0.4298	0.0137
$Bi_{0.95}Pr_{0.05}Fe_{0.97}Mn_{0.03}O_3$	-0.00014	0.1818	0.4299	0.0141
$Bi_{0.95}Pr_{0.05}Fe_{0.95}Mn_{0.05}O_3$	-0.00015	0.1819	0.4298	0.0147
$Bi_{0.9}Pr_{0.1}Fe_{0.9}Mn_{0.1}O_3$	-0.00019	0.1969	0.4544	0.0212
$Bi_{0.9}Pr_{0.1}Fe_{0.8}Mn_{0.2}O_3$	-0.00020	0.1967	0.4580	0.0220
$Bi_{0.8}Pr_{0.2}Fe_{0.9}Mn_{0.1}O_3$	-0.00021	0.1965	0.4701	0.0244
$Bi_{0.8}Pr_{0.2}Fe_{0.8}Mn_{0.2}O_3$	-0.00035	0.2268	0.4478	0.0440

Table 1 presents the crystal structure of the $BiFeO_3$ and $Bi_{1-x}Pr_xFe_{1-y}Mn_yO_3$ samples calculated using (Eq.2-4). Based on Table 1, the higher molar concentration of (Pr, Mn) leads to a smaller crystal size. The substitution of Bi by Pr and Fe by Mn causes a smaller crystal size because the dopants possess a smaller atomic radius[36]. Besides, the addition of (Pr, Mn) also enlarges the lattice strain of the $Bi_{1-x}Pr_xFe_{1-y}Mn_yO_3$ materials[37].

The UV-Vis spectrophotometer test gave the data of absorbance and transmittance, as presented in Fig. 2. Based on Fig. 2b, the absorbance spectra increase from $BiFeO_3$ sample to $Bi_{1-x}Pr_xFe_{1-y}Mn_yO_3$ samples, in which the increment occurs as the greater number of (Pr, Mn) dopants, especially at wavelengths of 200 nm to 400 nm or UV area. This means that the sample absorbs more UV light than visible light. Meanwhile, the transmittance spectra are the opposite of the absorbance spectra, where the values decrease with the higher concentration of (Pr, Mn) dopants. Thus, it denotes that more photons captured by $Bi_{1-x}Pr_xFe_{1-y}Mn_yO_3$ are transmitted than absorbed.

Furthermore, from Fig. 2, all film samples seem transparent and reveal a strong absorbance in the visible and UV regions. In the absorbance spectra (Fig. 2a), there is an inter-band transition, well-known as the adsorption edge, where the absorbance curve starts significantly dropping nearly to zero absorption at a particular wavelength (at about 370 – 400 nm in the figure). Figure 2a reveals that the co-doping process has moved the adsorption edge toward a longer wavelength due to the change in the crystallinity. Then, the adsorption edge relates to the bandgap energy, where its change reflects the modification of the optical bandgap of the film samples.

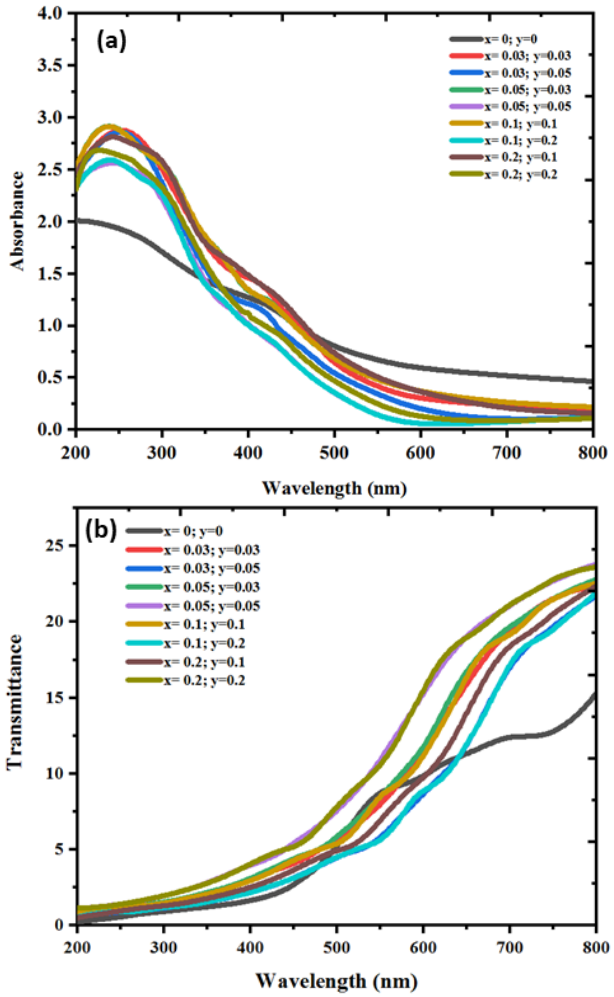

Fig. 2: (a) Absorbance and (b) transmittance spectra of $BiFeO_3$and $Bi_{1-x}Pr_xFe_{1-y}Mn_yO_3$

Figure 3 shows the refractive indices and the light dispersion energy of $BiFeO_3$ and $Bi_{1-x}Pr_xFe_{1-y}Mn_yO_3$ determined using the Swanepoel method (Eq. 5-7) and (Eq.8-10). From Fig. 3a, the refractive index was measured at 400 nm to 800 nm. The refractive index decreases as the concentration ratios of (Pr, Mn) dopants increase. In this study, (Pr, Mn) dopants cause a smaller unit cell volume. Consequently, the sample might only hold very few electrons. According to the Lorentz-Lorenz equation, if there are few electrons in the samples, the polarization will decrease so that the refractive index will

also decrease[38]. Meanwhile, as seen in Fig. 3b, the light dispersion is inversely proportional to the refractive index values[39].

Figure 4 presents the *I-V* curves of $BiFeO_3$ and $Bi_{1-x}Pr_xFe_{1-y}Mn_yO_3$ as the results of *I-V* characterization. Based on Fig. 4, the *I-V* curve is similar to the curve of the diode function. Table 3 lists the *I-V* characteristics of $BiFeO_3$ and $Bi_{1-x}Pr_xFe_{1-y}Mn_yO_3$. Based on Table 3, adding (Pr, Mn) into $BiFeO_3$ increases their solar cell's efficiency. It is considered because the ionic radius of the doped Pr^{3+} (0.99 Å) ions that replace Bi^{3+} (1.03 Å) and Mn^{2+} (0.48 Å) ions that replace Fe^{3+} (0.64 Å)[40] causes the unit cell volume to decline. The unit cell volume is in reverse with the spontaneous polarization, while the efficiency is proportionate with the spontaneous polarization. Thus, when the crystallite size shrinks, the spontaneous polarization increases, improving efficiency. Hence, the solar cell efficiency of $Bi_{1-x}Pr_xFe_{1-y}Mn_yO_3$ samples is enhanced with the higher (Pr, Mn) concentrations.

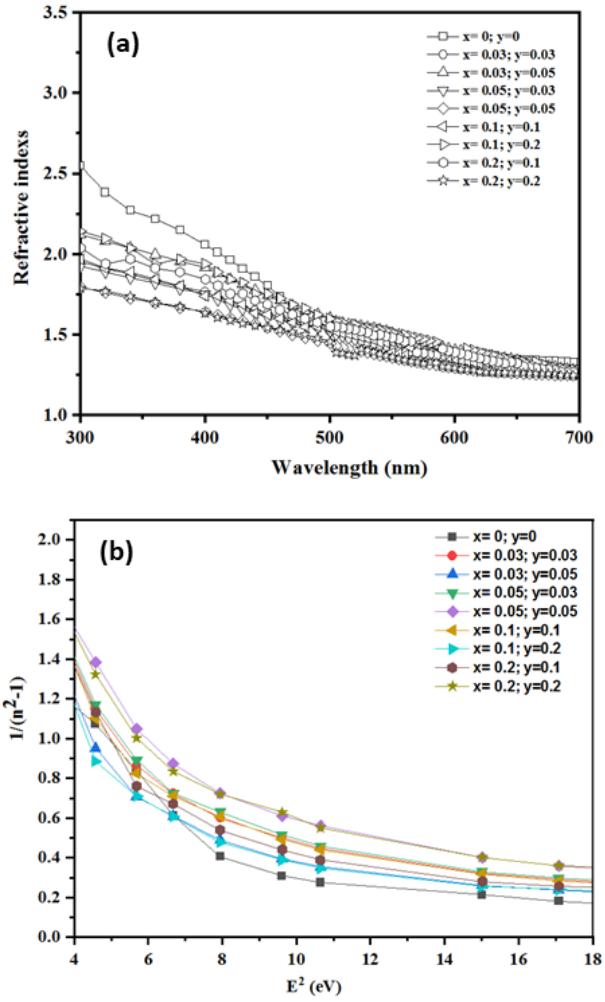

Fig. 3: (a) Refractive indices and (b) dispersion energy of $BiFeO_3$and $Bi_{1-x}Pr_xFe_{1-y}Mn_yO_3$

The strength of this study was that the synthesis of $BiFeO_3$ co-doped (Pr, Mn) using the CSD fabrication method and the investigation of the optical properties that remain scarce to be found currently. Therefore, the results of this study can be a reference for further related studies, especially for $BiFeO_3$ or other multiferroic materials. Furthermore, as an implication, this study's results can be a basic reference for the investigation of $BiFeO_3$ multiferroic materials for photovoltaic applications. This study, however, possesses limitations. First, it did not measure the bandgap energy in doped BFO samples for further optical properties. Besides, the electrical properties were only determined through I-V characteristics. Although it has indicated improved optical and electrical properties due to the doping treatment, further related tests must be performed, including energy gap measurements and other electrical property testing.

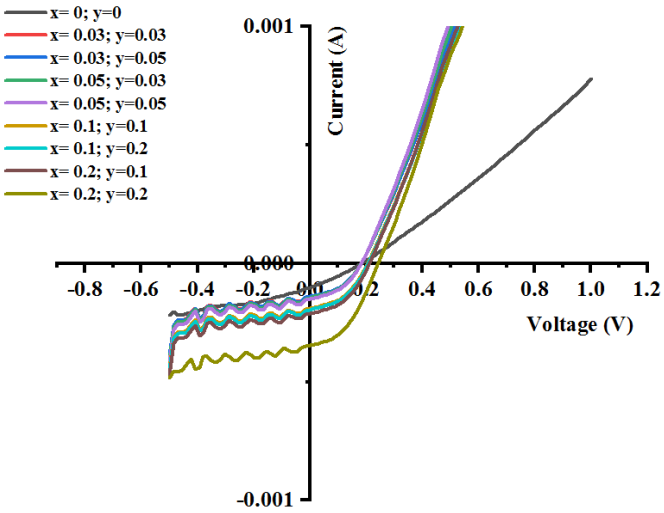

Fig. 4: I-V curves of $BiFeO_3$and $Bi_{1-x}Pr_xFe_{1-y}Mn_yO_3$

4. Conclusions

The synthesis of $BiFeO_3$ and $Bi_{1-x}Pr_xFe_{1-y}Mn_yO_3$ films grown on the substrate substrates has been successfully conducted via the CSD technique. The addition of (Pr, Mn) doping into $BiFeO_3$ shifted the diffraction peaks toward smaller angles, changing the crystal structure. The higher (Pr, Mn) concentration caused the decrement in the unit cell volume, lattice constants, crystal sizes, and the increment in the lattice strain. Meanwhile, the addition of (Pr, Mn) concentration caused the absorbance to increase and the transmittance to decrease, so the refractive index decreased while the light dispersion increased. Moreover, the addition of the (Pr, Mn) concentration ratio enhanced the I-V characteristics. Therefore, the addition of the (Pr, Mn) concentration ratio improved the crystal structure and optical and electrical characteristics of (Pr, Mn) co-doped $BiFeO_3$.

Acknowledgments

The authors thank Regular Fundamental Research Grants (Penelitian Fundamental Regular) No. 1280.1/UN27.22/PT.01.03/2023 for financing this research.

Conflict of interest

The authors state that no interest conflict is found in this research.

References

1) S. Hirata and M. Ohtaki, "Simultaneous Enhancement in the Electrical Conductivity and Reduction in the Lattice Thermal Conductivity Leading to Enhanced Thermoelectric ZT Realized by Incorporation of Metallic Nanoparticles into Oxide Matrix," *EVERGREEN,* **07** (01) 01-06 (2020). https://doi.org/10.5109/2740934
2) M. M. Rahman, S. Saha, M. Z. H. Majumder, T. T. Suki, M. H. Rahman, F. Akter, M. A. S. Haque, M. K. Hossain, "Energy Conservation of Smart Grid System Using Voltage Reduction Technique and Its Challenges," *EVERGREEN,* **09** (04) 924-938 (2022). https://doi.org/10.5109/6622879
3) Y. Yuan, Z. Xiao, B. Yang, and J. Huang, "Arising applications of ferroelectric materials in photovoltaic devices," *J. Mater. Chem.* **2** 6027–6041 (2014). DOI: 10.1039/c3ta14188h
4) N. A. Spaldin, S.W. Cheong, and R. Ramesh, "Multiferroics: Past, present, and future," *Phys. Today,* **63** (10) 38–43 (2010). doi:10.1063/1.3502547
5) C. Tablero, "Photovoltaic application of the multiferroic Bi_2FeCrO_6 double perovskite," *Sol. Energy,* **137** 173–178 (2016). https://doi.org/10.1016/j.solener.2016.08.004
6) W. Eerenstein, N. D. Mathur, and J. F. Scott, "Multiferroic and magnetoelectric materials," *Nature,* **442** (7104) 759–765 (2006). DOI: 10.1038/nature05023.
7) H. T. Yi, T. Choi, S. G. Choi, Y. S. Oh, and S.W. Cheong, "Mechanism of the Switchable Photovoltaic Effect in Ferroelectric $BiFeO_3$," *Adv. Mater.,* **23** (30) 3403–3407 (2011).
8) W. A. Wani, S. Kundu, K. Ramaswamy, and B. H. Venkataraman, "Optimizing phase formation of $BiFeO_3$ and Mn-doped $BiFeO_3$ nanoceramics via thermal treatment using citrate precursor method," *SN Appl. Sci.,* **2** 1969 (2020). https://doi.org/10.1007/s42452-020-03669-z
9) S. Pattanayak, A. Priyadarshan, R. Subudhi, R. K. Nayak, and R. Padhee," Tailoring of electrical properties of $BiFeO_3$ by praseodymium," *J. Adv. Ceram.,* **2** (3) 235–241 (2013). DOI: 10.1007/s40145-013-0065-x
10) Y. Iriani, M. D. Noviastuti, R. Suryana, D. K. Sandi, and D. Fasquelle, "Pr-doped $BiFeO_3$ thin films growth on quartz using chemical solution deposition," *Open Eng.,* **12** 447–452 (2022). https://doi.org/10.1515/eng-2022-0046
11) C. Cheng-Sao Chen, C. Pin-Yi, W. S. Chang, C. Blaise, Y. L. Hsieh, R. R. Chien, V. H. Schmidt, J. Yi-Shin Jou, and T. Chi-Shun, " Evolution of domain structure and ferroelectric polarization in praseodymium doped $BiFeO_3$ ceramics," *Mater. Res. Bull.,* **133** 111054 (2021). https://doi.org/10.1016/j.materresbull.2020.111054
12) A. Ghosh, D. P. Trujillo, H. Choi, S. M. Nakhmanson, S. P. Alpay, and Z. Jian-Xin, "Electronic and Magnetic Properties of Lanthanum and Strontium Doped Bismuth Ferrite: A First-Principles Study," *Sci. Rep.,* **9** 194 (2019).
13) X. Yi-Jun, G. Yi-Ping, D. Wen, G. Bing, L. Hua, and L. He-Zhou, "Preparation of La-doped $BiFeO_3$ Thin Film and Its Photovoltaic Properties," *J. Inorg. Mater.,* 28 (4) 436 – 440 (2013). DOI: 0.3724/SP.J.1077.2013.12298
14) K. S. Kumar, S. Ramu, A. Sudharani, M. Ramadhan, G. Murali, and R. P. Vijayalakshmi, "Enhanced magnetic and dielectric properties of Gd doped $BiFeO_3$: Er nanoparticles synthesized by sol-gel technique," *Physica E Low Dimens. Syst. Nanostruct.,* **115** 113689 (2020). https://doi.org/10.1016/j.physe.2019.113689
15) D. Feng, B. Huang, L. Li, X. Li, Y. Gu, W. Hu, and Z. Zhang, "The effects of Eu^{3+} doping on the epitaxial growth and photovoltaic properties of $BiFeO_3$ thin films," *J. Mater. Sci. Technol.,* 106 49 – 55 (2022). https://doi.org/10.1016/j.jmst.2021.07.025
16) M. N. Akhtar, M. Yousaf, M.A. Baqir, K. M. Batoo, and M. A. Khan, "Pr–Co co-doped BFO multiferroics nanomaterials for absorber applications," *Ceram. Int.,* **47** (2) 2144 – 2154 (2021). https://doi.org/10.1016/j.ceramint.2020.09.051
17) Y. Gu, Y. Zhou, W. Zhang, C. Guo, X. Zhang, J. Zhao, Y. Zhang, and H. Zheng, "Optical and magnetic properties of Sm-doped $BiFeO_3$ nanoparticles around the morphotropic phase boundary region," *AIP Adv.* **11** 045223 (2021). https://doi.org/10.1063/5.0042485
18) M. D. Noviastuti, Kusumandari, R. Suryana, Y. Iriani, and D. Fasquelle, "Effects of Nd and Mn Co-dopant on the Micro Structure and Optical Properties of $BiFeO_3$ Thin Films Elaborated by Chemical Solution Deposition (CSD)," *J. Phys.: Conf. Ser.,* **1825** (1) 012060 (2021). DOI:10.1088/1742-6596/1825/1/012060
19) J. K. Kim, S. S. Kim, W.J. Kim, A. S. Bhalla, and R. Guo, "Enhanced ferroelectric properties of Cr-doped $BiFeO_3$ thin films grown by chemical solution deposition," *Appl. Phys. Lett.,* **88** (13) 132901 (2006). https://doi.org/10.1063/1.2189453
20) L. Xia-Li and D. Jian-Qing, "Prominent ferroelectric properties in Mn-doped $BiFeO_3$ spin-coated thin films," *J. Alloys Compd.,* **886** 161168 (2021). https://doi.org/10.1016/j.jallcom.2021.161168
21) P. He, Z. L. Hou, C.Y. Wang, Z.J. Li, J. Jing, and S. Bi, "Mutual promotion effect of Pr and Mg co-substitution on structure and multiferroic properties of $BiFeO_3$ ceramic," *Ceram. Int.,* **43** (1) 262–267 (2017). https://doi.org/10.1016/j.ceramint.2016.09.148

22) X. Deng, Z. Zeng, R. Gao, Z. Wang, G. Chen, W. Cai, and C. Fu, " Study of structural, optical and enhanced multiferroic properties of Ni doped BFO thin films synthesized by sol-gel method," *J. Alloys Compd.,* **831** 154857 (2020). https://doi.org/10.1016/j.jallcom.2020.154857
23) M. Sajjad, S. Aslam, K. Ali, Y. Jamil, H. M. Khan, M. R. Ahmad, M. Z. Rashid, and M. Alzaid," Enhanced structural and optical properties of Mn-doped $BiFeO_3$ nanoparticles at different substitutions," *J. Optoelectron. Adv. Mater.,* **23** (3-4) 199 – 206 (2021).
24) F. Yan, M. O. Lai, L. Lu, and Z. Tie-Jun, "Enhanced Multiferroic Properties and Valence Effect of Ru-Doped $BiFeO_3$ Thin Films," *J. Phys. Chem. C* **114** (15) 6994–6998 (2010). https://doi.org/10.1021/jp1009127
25) S. K. Singh, H. Ishiwara, K. Sato, and K. Maruyama, "Microstructure and frequency-dependent electrical properties of Mn-substituted $BiFeO_3$ thin films," *J. Appl. Phys.,* **102** (9) 094109 (2007). https://doi.org/10.1063/1.2812594
26) Y. Iriani, R. Afriani, D. K. Sandi, and F. Nurosyid, Co-precipitation Synthesis and Photocatalytic Activity of Mn-doped $SrTiO_3$ for the Degradation of Methylene Blue Wastewater," *EVERGREEN*, **09** (04) 1039-1045 (2022). https://doi.org/10.5109/6625717
27) M. Egiza, H. Naragino, A. Tominaga, K. Murasawa, H. Gonda, M. Sakurai, and T. Yoshitake, "Si and Cr Doping Effects on Growth and Mechanical Properties of Ultrananocrystalline Diamond/Amorphous Carbon Composite Films Deposited on Cemented Carbide Substrates by Coaxial Arc Plasma Deposition," *EVERGREEN,* **03** (01) 32-36 (2016). https://doi.org/10.5109/1657738
28) K. Taira and H. Einaga," Distribution Ratio of Pt on Anatase and Rutile TiO_2 Particles, Determined by X-ray Diffraction and Transmission Electron Microscopy Analysis of Pt/TiO_2(P25)." *EVERGREEN,* **05** (04) 13-17 (2018). https://doi.org/10.5109/2174853
29) A. Khorsand Zak, W. H. Abd. Majid, M. E. Abrishami, and R. Yousefi, "X-ray analysis of ZnO nanoparticles by Williamson–Hall and size–strain plot methods," *Solid State Sci.,* **13** (1) 251–256 (2011). DOI:10.1016/j.solidstatesciences.2010.11.024
30) Birkholz M., Thin Film Analysis by X-ray Scattering Wiley-VCH Verlag GmbH and Co. KGaA, Weinheim (2006).
31) R. Swanepoel, "Determination of the thickness and optical constants of amorphous silicon," *J. Phys. E: Sci. Instrum.,* **16** (12), 1214 (1983). DOI: 10.1088/0022-3735/16/12/023
32) R. Swanepoel, "Determination of surface roughness and optical constants of inhomogeneous amorphous silicon films," *J. Phys. E: Sci. Instrum,.* **17** (10), 896 (1984). DOI: 10.1088/0022-3735/17/10/023.
33) M. Santika, Y. Iriani, and R. Suryana, "Influence of Thickness on Optical Properties of Bismuth Ferrite Layers Grown on Quartz Substrates by Chemical Solution Deposition," *Mater. Today: Proc.,* **13** (1) 82–86 (2019). https://doi.org/10.1016/j.matpr.2019.03.192
34) S. Arti, P. Kumar, R. Kumar, P. Walia, and V. Verma, "Improved ferroelectric, magnetic and photovoltaic properties of Pr doped multiferroic bismuth ferrites for photovoltaic application," *Results Phys.,* **14** 102403 (2019). https://doi.org/10.1016/j.rinp.2019.102403
35) M. S. Alkathy and K. C. James Raju, "Structural, dielectric, electromechanical, piezoelectric, elastic and ferroelectric properties of lanthanum and sodium co-substituted barium titanate ceramics," *J. Alloys Compd.,* **737** 464–476 (2018). DOI:10.1016/J.JALLCOM.2017.12.121
36) Y. Wang, K. Miao, W. Wang, and Y. Qin, "Fabrication of lanthanum doped $BaTiO_3$ fine-grained ceramics with a high dielectric constant and temperature-stable dielectric properties using hydro-phase method at atmospheric pressure," *J. Eur. Ceram. Soc.,* **37** 2385–2390 (2017).
37) D. Kumar, M. Singh, and A.K. Singh, "Crystallite size effect on lattice strain and crystal structure of $Ba_1/4Sr_3/4MnO_3$ layered perovskite manganite, "*AIP Conf. Proc.,* **1953** (1) 030185 (2018). DOI:10.1063/1.5032520
38) L. Ciabini, M. Santoro, R. Bini, and V. Schettino, "High-Pressure Photoinduced Ring Opening of Benzene," Physical Review Letters, **88** (8) 085505 (2002). DOI: 10.1103/PhysRevLett.88.085505
39) A.M. Abdelghany, E.M. Abdelrazek, S.I. Badr, and M.A. Morsi, "Effect of gamma-irradiation on (PEO/PVP)/Au nanocomposite: Materials for electrochemical and optical applications," Materials and Design, **97** 532 – 543 (2016). http://dx.doi.org/10.1016/j.matdes.2016.02.082
40) D. Varshney, P. Sharma, S. Satapathy, and P. K. Gupta, "Structural, magnetic and dielectric properties of Pr-modified $BiFeO_3$ multiferroic," *J. Alloys and Compd.,* **584** 232–239 (2014). http://dx.doi.org/10.15446/dyna.v87n215.83538